Eur Biophys J (2005) 34: 82–90
DOI 10.1007/s00249-004-0427-y

ARTICLE

**Andrew H. A. Clayton · Nectarios Klonis
Stephen H. Cody · Edouard C. Nice**

Dual-channel photobleaching FRET microscopy for improved resolution of protein association states in living cells

Received: 19 January 2004 / Revised: 26 May 2004 / Accepted: 28 May 2004 / Published online: 30 June 2004

Abstract Fluorescence resonance energy transfer (FRET) from a donor-labelled molecule to an acceptor-labelled molecule is a useful, proximity-based fluorescence tool to discriminate molecular states on the surface and in the interior of cells. Most microscope-based determinations of FRET yield only a single value, the interpretation of which is necessarily model-dependent. In this paper we demonstrate two new measurements of FRET heterogeneity using selective donor photobleaching in combination with synchronous donor/acceptor detection based on either (1) full kinetic analysis of donor-detected and acceptor-detected donor photobleaching or (2) a simple time-based ratiometric approach. We apply the new methods to study the cell surface distribution of concanavalin A yielding estimates of FRET and non-FRET population distributions, as well as FRET efficiencies within the FRET populations.

Keywords Oligomerisation · Fluorescein · Rhodamine · Fluorescence resonance energy transfer (FRET) · Protein interactions · Two-component analysis

Introduction

Macromolecular oligomerisation and conformation are key biological control mechanisms that determine the activity of functional biological molecules. In cellular systems an additional level of control is provided through the spatial and temporal partitioning of biochemical reactions. Determination of the relevant reaction state(s) inside cells requires fluorescence methodologies that are sensitive to molecular interactions on the nanometre scale and can provide spatial resolution on the length scales relevant to the cell, i.e. the micron scale. These requirements are met by exploiting the photophysical properties of fluorescently tagged proteins introduced or expressed into the cell in combination with fluorescence microscopy techniques (Bastiaens and Jovin 1996; Jares-Erijman and Jovin 2003).

Fluorescence resonance energy transfer (FRET) is one widely employed fluorescence tool to discriminate molecular states on the surface and in the interior of cells. Its utility derives from its exquisite sensitivity to molecular separation; the rate of energy transfer between a donor label and an acceptor label decreases with the inverse sixth power of molecular separation at typical length scales of 1–10 nm. Thus, the energy transfer efficiency can be used as a spectroscopic ruler (Stryer and Haugland 1967) and for quantitative determinations of molecular proximity and intermolecular interactions (Selvin 2000) including protein–protein interactions (Gadella and Jovin 1995; Szollosi et al. 2002), protein–DNA interactions (Millar 2000), protein–membrane interactions and the three-dimensional structure of molecules (Clegg et al. 1993; dos Remedios and Moens 1995; Klostermeier and Millar 2001–2002).

FRET introduces an additional pathway for deactivation of the excited state of the donor molecule and thereby causes a decrease in the donor excited-state lifetime, donor fluorescence quantum yield and donor photobleaching rate. FRET causes an increase in the emission of fluorescent acceptor molecules excited via the donor. Experimental approaches for determining the energy-transfer efficiency exploit these changes in the photophysics of the donor and acceptor molecules. In commercially available wide-field and confocal microscopes, the most popular means of detecting FRET in the steady-state are through ratiometric

A. H. A. Clayton (✉) · S. H. Cody · E. C. Nice
Ludwig Institute for Cancer Research,
Royal Melbourne Hospital, P.O. Box 2008,
3050 Parkville, Victoria, Australia
E-mail: Andrew.Clayton@ludwig.edu.au

N. Klonis
Department of Biochemistry, La Trobe University,
3086 Melbourne, Victoria, Australia

intensity measurements (Gordon et al. 1998; Hoppe et al. 2002) or photobleaching methods (Jovin and Arndt-Jovin 1989; Bastiaens et al. 1996) in which either the donor or acceptor molecule is selectively photodestructed. FRET derived from monitoring the decrease in the nanosecond decay time of fluorophores in single-channel or imaging modes is an alternative and elegant approach but requires specialised instrumentation. Most microscope-based measurements yield an apparent single FRET efficiency (per cell or image pixel), the interpretation of which is necessarily model-dependent. However, particularly in the cellular milieu, an understanding of the heterogeneity in macromolecular conformation and association is of paramount importance.

Cellular studies of the transfer efficiency as a function of acceptor labelling density, donor-to-acceptor labelling ratio, label radius or cell size (Kubitscheck et al. 1993; Kenworthy and Edidin 1998; Szollosi et al. 2002) can give information on the type of molecular interactions present and whether they arise from a random distribution of molecules, a clustering of molecules or a partially clustered distribution. Measurements can establish not only the nature of the distribution being studied, but are also sensitive to changes in the distribution under physical (e.g. space, time, temperature) and biological perturbations (external stimuli). In this regard, standard transfer-efficiency measurements are often difficult to interpret because changes in the FRET efficiency can be related to the degree of association or to the geometry of the associated complex. It would be desirable to have a method that can measure the proportions of associated and unassociated molecules and the FRET efficiency (conformation) within the associated population independently. To this end we offer a new FRET method that greatly extends the capabilities of current FRET techniques.

In this paper we demonstrate the measurement of FRET heterogeneity using selective donor photobleaching in combination with synchronous donor/acceptor detection. In the donor photobleach method an indirect measure of the fluorescence lifetime of a fluorophore (Hirschfeld 1976) is provided by measuring the donor photobleaching kinetics. The rate of irreversible photobleaching of the donor fluorophore is conventionally measured in the microscope by monitoring the loss (or fading) of donor fluorescence upon continuous or repetitive illumination (Fig. 1A). In the presence of FRET to a proximal energy acceptor, the rate of photobleaching of donor molecules is decreased (Fig. 1B; Jovin and Arndt-Jovin 1989). The photodestruction of a donor molecule within a donor–acceptor FRET pair (or complex) can also be measured from the loss in sensitized-acceptor fluorescence because the donor and acceptor form a coupled system. This provides a very specific measure of FRET within the donor–acceptor ensemble, provided the acceptor itself is not photochemically depleted during this process (photolabile donor/photostable acceptor). It follows

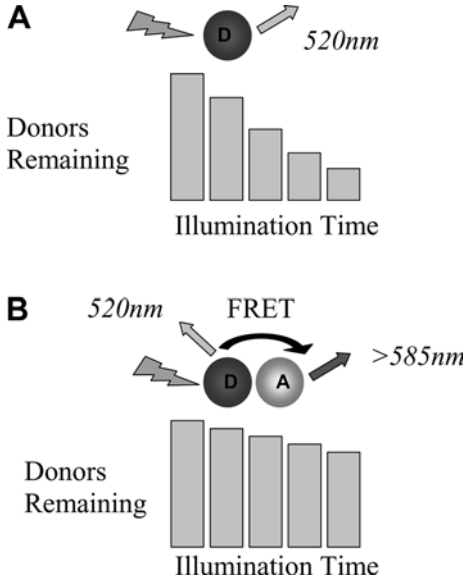

Fig. 1A, B Photobleaching microscopy and FRET. **A** Constant or repetitive illumination of a fluorophore leads to photochemical destruction of the fluorophore. The steady-state fluorescence intensity as a function of illumination time can be used to monitor the kinetics of the photobleaching process, the rate of which is proportional to the fluorescence lifetime of the fluorophore. **B** Under conditions of FRET, the rate of photobleaching of the donor fluorophore decreases and some of the excitation energy from the donor appears as acceptor fluorescence. For a coupled donor–acceptor FRET pair, the photobleaching rate can be measured either from the donor fluorescence or from the sensitized-acceptor fluorescence, provided the acceptor is photostable and the donor photolabile. Wavelengths indicate approximate wavelengths of observation of fluorescein and rhodamine fluorescence

that, in a complex system involving a distribution of FRET states, the donor-detected photobleaching kinetics will provide a measurement that includes all donor molecules (FRET and non-FRET) while the acceptor-sensitized emission-detected donor photobleaching will provide a measurement that includes only the FRET population. Combining the donor emission- and acceptor emission-detected measurements gives greater insight into the spatial distribution of macromolecules in complex assemblies.

To provide a concrete example of the application of the method and theory we present photokinetic FRET measurements of fluorescein-conjugated concanavalin A and rhodamine-conjugated concanavalin A bound to cell-surface glycoproteins of LIM1215 colon carcinoma cells (Whitehead et al. 1985). ConA is a lectin that binds primarily to glycoproteins and glycolipids containing D-glucose- and D-mannose and has been used as a model system for examining receptor aggregation. Our results show that the lectin receptors are neither randomly distributed nor homogeneously clustered. The data suggest that at least two-thirds of the lectin receptors are in close proximity on the cell surface with the clustered population exhibiting a transfer efficiency of 70%. Moreover, from comparison of data analysed from

complete photobleaching and partial photobleaching, we show that protein conformation or protein association can be mapped on living cells using only two images from a time series of dual-channel detected fluorescence images. This extended photobleaching FRET method is applicable to any fluorescence microscope with dual- or multi-channel acquisition and has the ability to provide quantitative insight into donor–acceptor distance distributions in living cells.

Materials and methods

Fluorescein isothiocyanate-conjugated concanavalin A (FITC-conA) and tetramethylrhodamine isothiocyanate-conjugated concanavalin A (TRITC-conA) were purchased from Molecular Probes (Oregon, USA). Solutions containing varying proportions of FITC-conA and TRITC-conA up to a total constant conA concentration of 500 μg/ml were made up in phosphate-buffered saline (PBS). LIM1215 human colon carcinoma cells were grown to subconfluency on glass coverslips in Delbucco's medium (supplemented with 10% fetal calf serum). The coverslips were placed in a specimen chamber (Sykes and Moore 1959) and transferred to an incubation chamber held at 37 °C in an atmosphere of 5% CO_2. After a 15-min incubation with FITC-conA and/or TRITC-conA solutions [acceptor-to-donor (A:D) molar ratios of 0, 1.5, 3, at constant total concentration of 50 μg/ml], the cells were rinsed three times with PBS and then imaged using a BIORAD MRC 1000 scanning fluorescence confocal microscope (Nikon Plan Apo, 60X NA 1.2 water immersion lens, zoom = 3, pinhole = 4, Kalman average = 3) with dual-channel detection (channel 1, FITC, ex 488 nm, emission 520/22-nm bandpass; channel 2, FRET, ex 488 nm, 585 long pass). Sixty images were acquired and stored as a time series for image processing. The cross-talk contribution (see Theory section; $S_{ch1} = 0.66$), representing spillage of donor emission into the acceptor FRET channel, was determined by measuring samples labelled donor-only. All data collected in the FRET channel were corrected for this effect.

The photobleaching series were analysed using two approaches as outlined in the Theory section. In the first approach, regions of interest on the cell membrane were selected (20×20 pixel area) and the average intensity value versus image number was extracted (Image-J), plotted, and fit to an exponential + baseline function (Excel). The extracted time constants [Eq. (4)] were used in the calculation of energy-transfer efficiencies and fractional population of FRET species according to Eqs. (6) and (7). In the second approach, a constant background was subtracted from each intensity value, and the ratio of the intensities of the fifth and first image in the time series was used to compute effective time constants, transfer efficiencies and populations according to Eqs. (11), (12), (13), and (14).

Theory

Bimodal discrete distribution model (FRET and non-FRET population model)

We assume a two-state model that attributes the fluorescence from a donor-labelled population as due to a contribution from donors not undergoing FRET and a distinct population that undergoes FRET. The intensity decay detected in the donor emission channel (ch1) due to photobleaching will decay biexponentially due to the presence of two populations,

$$I^{ch1}(t) = A_f^{ch1}\, e^{(-t/\tau_f)} + A_{nf}^{ch1}\, e^{(-t/\tau_{nf})} \quad (1)$$

where τ_f and A_f depict the time constant and amplitude characterising the FRET population and τ_{nf} and A_{nf} depict the corresponding non-FRET values. By definition, $\tau_f > \tau_{nf}$ because energy transfer depopulates the donor excited state causing a reduction in excited-state lifetime and photobleaching rate. τ_{nf} is determined separately using a donor-only labelled sample. Using dual-channel detection, the acceptor emission (ch2) can also be synchronously measured yielding the following time dependence:

$$I^{ch2}(t) = S_{ch1}\left(A_f^{ch1} e^{(-t/\tau_f)} + A_{nf}^{ch1} e^{(-t/\tau_{nf})}\right) + S_{ch3} I^{ch3} + A_f^{FRET} e^{(-t/\tau_f)} \quad (2)$$

where, S_{ch1} is a constant representing cross talk of donor emission into the acceptor channel, $S_{ch3}I_{ch3}$ represents the contribution of acceptor emission that is directly excited and $A_f{}^{FRET}e^{(-t/\tau f)}$ represents the decay of acceptor-sensitized emission due to loss of donor molecules by photobleaching. Note that in the case of a completely photostable acceptor, the contribution of directly excited acceptor molecules does not vary with time and appears as a constant term in Eq. (2). In the case of the FITC/TRITC pair, the FITC is easily photobleached and the sensitized-emission term in Eq. (2) is expected to decay much faster than the intrinsic decay of TRITC due to photobleaching. Under our illumination and collection conditions, the rate of TRITC photobleaching is 5% of the FITC photobleaching rate (data not shown), in accord with previous observations (7%; Young et al. 1994). Thus the photobleaching of directly excited TRITC does not interfere with sensitized-emission rate-constant determinations. Eqs. (1) and (2) are both double exponential functions but with shared time constants.

The common parameters in Eqs. (1) and (2) invite the possibility that a two-channel global analysis with linked lifetimes will yield the desired parameters. However, global analysis works optimally in cases where the system is *overdetermined*, which is not the case here. Therefore we offer two alternative approaches that are simpler to implement and analyse. In the first approach, Eqs. (1) and (2) are transformed into effective single

exponential functions, from which all the required parameters can be determined. In the second approach, a simple time ratio is used, which allows for repeated determinations in live-cell imaging and facile image processing.

Use of effective exponential functions to estimate populations and FRET efficiencies. The time-integral lifetime approach

Following Gadella and Jovin (1995), we begin by rewriting Eq. (1) in terms of population fractions (which are normalized to unity)

$$I^{\mathrm{ch1}}(t) = \chi_{\mathrm{f}}(\tau_{\mathrm{nf}}/\tau_{\mathrm{f}})\exp(-t/\tau_{\mathrm{f}}) + (1-\chi_{\mathrm{f}})\exp(-t/\tau_{\mathrm{nf}}) \quad (3)$$

where χ_{f} is the fractional population of molecules undergoing FRET and (1-χ_{f}) is the fraction of molecules not undergoing FRET.

Equation (3) can be rewritten as an effective exponential (baseline subtracted or determined in the fitting),

$$I^{\mathrm{ch1}}(t) = A_{\mathrm{f}}\exp(-t/\tau_{\mathrm{eff}}) \quad (4)$$

Similarly, Eq. (2) can be transformed to a simple exponential decay by subtraction of the relevant cross-talk terms,

$$I^{\mathrm{ch2}}(t) - S_{\mathrm{ch1}}I^{\mathrm{ch1}}(t) = A_{\mathrm{f}}^{\mathrm{FRET}}\exp(-t/\tau_{\mathrm{f}}) + S_{\mathrm{ch3}}I^{\mathrm{ch3}} \quad (5)$$

The relationship between χ_{f} and the lifetimes, τ_{eff}, τ_{f}, and τ_{nf}, is found by minimising the sum of the variance between Eqs. (3) and (4). The analytical result determined previously by Gadella and Jovin (1995) is

$$\chi_{\mathrm{f}} = \left(\alpha^2\beta + 1\right)^{-1} \quad (6)$$

where $\alpha = (\tau_{\mathrm{nf}} + \tau_{\mathrm{eff}})/(\tau_{\mathrm{f}} + \tau_{\mathrm{eff}})$ and $\beta = (\tau_{\mathrm{f}} - \tau_{\mathrm{eff}})/(\tau_{\mathrm{eff}} - \tau_{\mathrm{nf}})$. The χ_{f} value obtained in this manner is a lower bound (Gadella and Jovin 1995).

The transfer efficiency determined from the kinetics of sensitized emission is given by

$$E = 1 - \tau_{\mathrm{nf}}/\tau_{\mathrm{f}} \quad (7)$$

Use of time-ratio functions to estimate populations and FRET efficiencies—the time-derivative lifetime approach

In some instances, the recording of the complete bleaching curve is impractical, for example in live-cell imaging, where a change in cell morphology or in the spatial distribution of fluorophores during the long exposure times for photobleaching will cause problems with image registration, and in some cases produce unwanted physiological artefacts. A simpler approach is to utilise the natural photobleaching that occurs with replicate image acquisition, using the information contained in a single partial bleach step or serious of steps.

Let R^{DA} be equal to the ratio of total post-bleach to total pre-bleach intensities in the donor channel, reflecting a contribution from the complexed and uncomplexed species.

$$R^{\mathrm{DA}} = \left[I^{\mathrm{ch1}}(t_2)/I^{\mathrm{ch1}}(t_1)\right]^{\mathrm{DA}} \quad (8)$$

Let the ratio of post- to pre-bleach intensity for donor-only sample be equal to

$$R^{\mathrm{D}} = \left[I^{\mathrm{ch1}}(t_2)/I^{\mathrm{ch1}}(t_1)\right]^{\mathrm{D}} \quad (9)$$

Let the ratio of post- to pre-bleach intensity for donor–acceptor complexes determined from the drop in sensitized FRET emission be:

$$R^{\mathrm{FRET}} = \left[I^{\mathrm{ch2}}(t_2) - S_{\mathrm{ch1}}I^{\mathrm{ch1}}(t_2)\right]/\left[I^{\mathrm{ch2}}(t_1) - S_{\mathrm{ch1}}I^{\mathrm{ch1}}(t_1)\right] \quad (10)$$

For short photobleaching times, i.e. $(t_2-t_1) \to 0$, the series expansion for exponential functions can be truncated to derive a simple expression for the apparent photobleaching lifetime, via $R = \exp[(t_2-t_1)/\tau] \approx 1-[(t_2-t_1)/\tau]$, yielding:

$$\tau_{\mathrm{f}} = (t_2 - t_1)/\left(1 - \left(R^{\mathrm{FRET}}\right)\right) \quad (11)$$

The lifetime defined is this manner is essentially the time derivative and thus measures the initial speed of the decay.

Provided the time interval between pre- and post-bleach images is a constant for the different donor-only and donor–acceptor samples, the transfer efficiency (E) within the FRET population is given by:

$$\begin{aligned} E_{\mathrm{FRET}} &= 1 - (\tau_{\mathrm{nf}}/\tau_{\mathrm{f}}) \\ &= 1 - \left[\left(1 - R^{\mathrm{FRET}}\right)/\left(1 - R^{\mathrm{D}}\right)\right] \end{aligned} \quad (12)$$

An apparent transfer efficiency derived from the donor emission channel photokinetics, E_{DA}, is defined similarly:

$$\begin{aligned} E_{\mathrm{DA}} &= 1 - (\tau_{\mathrm{nf}}/\tau_{\mathrm{f}}) \\ &= 1 - \left[\left(1 - R^{\mathrm{DA}}\right)/\left(1 - R^{\mathrm{D}}\right)\right] \end{aligned} \quad (13)$$

The fluorescence fraction of molecules undergoing FRET is given by

$$F_{\mathrm{f}} = E_{\mathrm{DA}}/E_{\mathrm{FRET}} \quad (14)$$

The advantage of this approach is that repeated determinations can be made and the determinations are less dependent on background since the measurements are made before significant photobleaching of the sample has occurred.

Results and discussion

ConA distribution associated with living LIM1215 colon carcinoma cells

The distribution of FITC-conA on living LIM1215 colon carcinoma cells was primarily associated with the

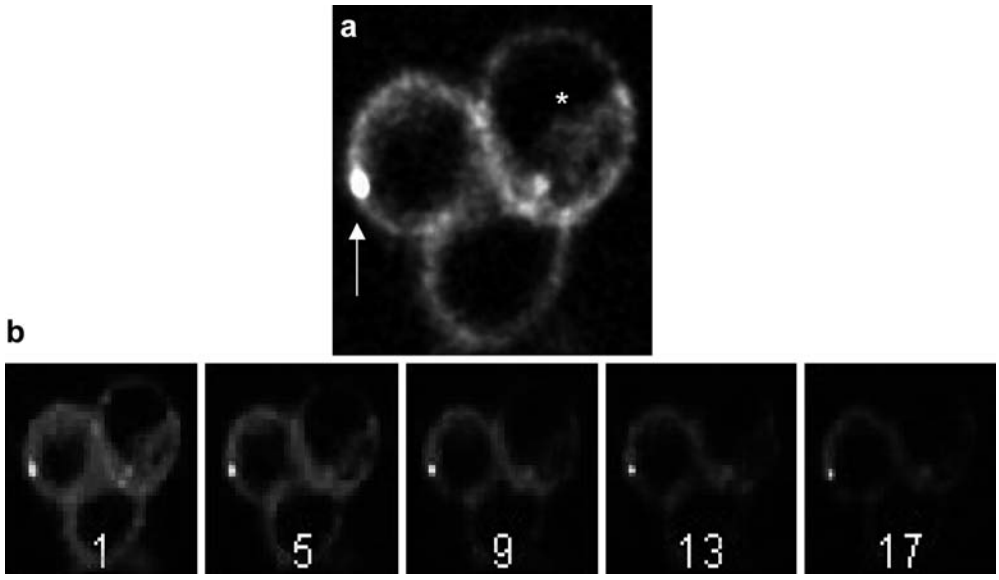

Fig. 2 a Confocal laser-scanning microscopy image of FITC-conA-stained LIM1215 human colon carcinoma cells showing the distinctive staining of the cellular plasma membranes. *Arrow* Patch of conA receptors, *asterisk* internalised conA. **b** Time series of cell presented in **a** showing the progressive photobleaching of fluorescein fluorescence upon replicate image acquisition (images labelled according to image number). Images *1* and *5* represent typical images used to compute the time-ratio lifetimes

plasma membrane as shown by confocal laser scanning microscopy (Fig. 2a) Some cells showed visible patching (Fig. 2a, arrow) and internalisation of the conA (Fig. 2a, asterisk). Our analyses were confined to regions of interest on the cell surface. Synchronous dual-channel photobleaching FRET measurements were performed on conA fluorescein-labelled donor and conA rhodamine-labelled acceptor molecules bound to live LIM1215 colon carcinoma cells. As expected, replicate image acquisition resulted in substantial photobleaching of the fluorescein fluorophore as shown in the time series of images presented in Fig. 2b. Typical time traces of the photobleaching of the fluorescein-conA (observed through the fluorescein channel) at different labelling molar ratios are shown in Fig. 3a (logarithmic scale). It is evident from the curves presented in Fig. 3a that addition of the rhodamine acceptor caused an appreciable decrease in the rate of photobleaching of the fluorescein label, consistent with energy transfer between the conA-labelled surface glycoproteins. The mean decay time of the donor determined from an exponential fit in the absence of acceptor was 11 s, and increased progressively from 16 s at an acceptor-to-donor (A:D) molar ratio of 1.5:1 to 20 s at a molar ratio of 3:1. The corresponding kinetics of acceptor-detected donor photobleaching of the 3:1 molar ratio labelled cells, together with the kinetics of the donor channel emission are shown in Fig. 3b. It is evident that the decay of the acceptor-detected donor emission was significantly longer-lived than that of the donor channel. The acceptor-detected donor photobleaching is characterised with a time constant of approximately 40 s. This value is longer than the donor-detected time constants but significantly shorter than the time constant for direct photobleaching of the acceptor of 150–250 s [based on it

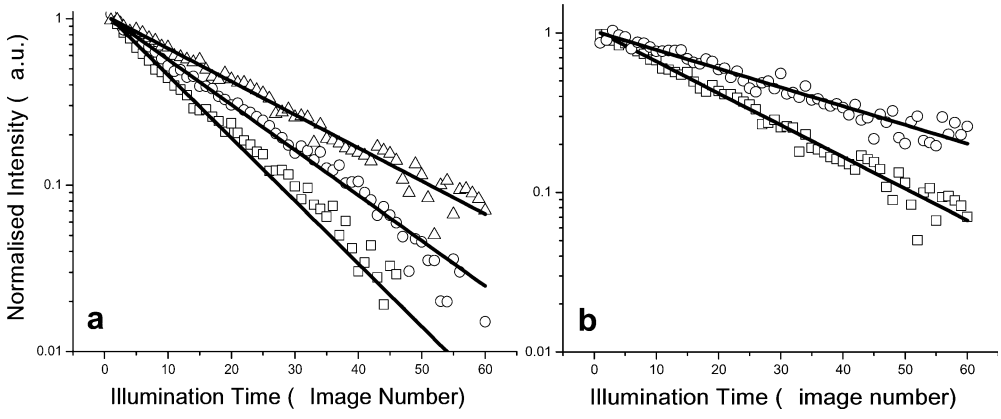

Fig. 3 a Donor-detected photobleaching curves of FITC-conA on the surface of LIM1215 human colon carcinoma cells as a function of added acceptor TRITC-conA. *Data points* denote the baseline-subtracted and normalised experimental values. A:D molar ratios: *triangles* 3:1, *circles* 1.5:1, *squares* 0. The *solid lines* are exponential fits to the data. Note the progressive decrease in photobleaching rate as the proportion of added TRITC-conA acceptor is increased. **b** Comparison of donor-detected (*squares*) and acceptor-detected (*circles*) normalised photobleaching curves of FITC-conA on the surface of LIM1215 human colon carcinoma cells at A:D molar ratio = 3:1. *Solid lines* are fits to the data. The distinctly different photobleaching kinetics are indicative of heterogeneity of energy transfer

Table 1 Photobleaching time constants, fractional FRET populations and FRET efficiencies obtained from analysis of dual-channel photobleaching FRET measurements of FITC-conA and TRITC-conA bound to living LIM1215 colon carcinoma cells

Label ratio (A:D molar ratio)	Method	Donor channel lifetime[a]	FRET channel lifetime	χ_f(%)	E (%)
0:1	Exponential	11 ± 2	N/A	N/A	N/A
0:1	Time ratio	11 ± 2	N/A	N/A	N/A
1.5:1	Exponential	16 ± 3	41 ± 6	47	73
1.5:1	Time ratio	15 ± 3	39 ± 7	65	72
3:1	Exponential	21 ± 5	37 ± 7	68	70
3:1	Time ratio	20 ± 5	42 ± 8	87	73

[a]The values (mean ± SE) correspond to the mean of at least ten determinations corresponding to regions of interest (20×20 pixels) on the cell surface

being 5–7% of the FITC bleaching rate (data not shown; Young et al. 1994)]. Thus the loss in intensity of the acceptor emission from donor excitation occurred through the bleaching of donor molecules participating in FRET. Similar acceptor-detected donor photobleaching rates were observed for the 1.5:1 stoichiometry population. The mean and standard deviations in the time constants derived from the fits of selected regions of interest (> 10) using both the exponential-fit and time-ratio methods are collected in Table 1.

In comparing the results from the exponential-fit and time-ratio approaches, good agreement is seen in the extracted time constants and in the derived transfer efficiencies. With regard to the time-ratio approach, important advantages are the small number of images required (minimum of two), the facile image processing (simple division, addition) and retention of spatial information. In cases where no spatially correlated FRET occurs, such as the situation here, the large number of pixels generated in an image allows the distribution of transfer efficiencies and fractional populations to be determined from a large number of observations. Examples of population (Fig. 4a) and FRET distributions (Fig. 4b) from the time-ratio approach are shown in Fig. 4. It is notable that the mean population fraction of FRET molecules and mean transfer efficiency obtained from these distributions (90 and 76%) agree well with the data listed in Table 1, i.e. from the full kinetic analysis approach (87 and 73%). We conclude that the dual-channel detected time-ratio approach is useful and applicable to FRET microscopy investigations.

The disparity between the donor-detected and acceptor-detected photobleaching kinetics is evidence that the donor and acceptor probes experience a distribution of distances on the cell surface on the time scale of the measurement. The donor-detected emission kinetics will be weighted towards the more fluorescent and faster photobleaching molecules in the distribution (smaller FRET efficiencies including donors not undergoing FRET), while the sensitized emission kinetics will be dominated by acceptor molecules that have undergone significant FRET (smaller donor–acceptor separations). The interpretation used here in terms of simplest FRET/non-FRET population model assigns to the non-FRET population the donor molecules that are too distant from acceptor-labelled molecules to yield

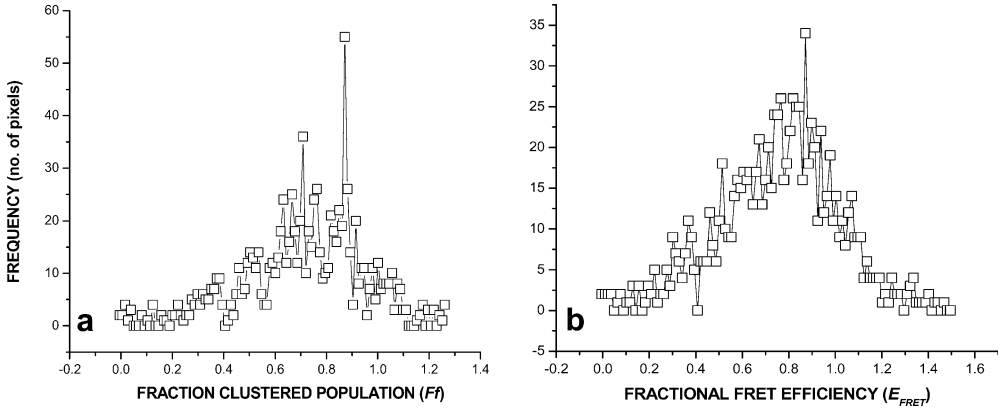

Fig. 4 **a** Population distribution of clustered protein calculated from time-ratio approach. *Squares* indicate data points. The mean fractional fluorescence due to clustered protein was 70%, corresponding to a mean molar fraction of clustered protein of 90%. The FRET maps used to obtain the histogram were generated from the time ratio of two acceptor-detected and two donor-detected donor-photobleaching images of FITC-conA on the surface of LIM1215 human colon carcinoma cells at a TRITC-conA to FITC-conA molar ratio of 3:1. **b** Distribution of FRET efficiencies calculated from time-ratio approach. *Squares* indicate data points. The mean transfer efficiency was 76%. The FRET map used to obtain the histogram was generated from the time ratio of two acceptor-detected donor-photobleaching images of FITC-conA on the surface of LIM1215 human colon carcinoma cells at a TRITC-conA to FITC-conA ratio of 3:1

measurable energy transfer (i.e. greater than 10 nm, unclustered) and another population of donor molecules that are proximal to acceptors (i.e. at distances less than 10 nm and probably in clusters). The parameters corresponding to this model are shown in Table 1. The data collected at the highest acceptor-to-donor labelling ratio are consistent with a fraction-clustered protein of 68–87% and an average efficiency of transfer of 73% within the clustered fraction. An estimate of the true level of clustered protein can be determined from the dependence of the clustered fraction on labelling stoichiometry. By linear extrapolation of the fractional clustering (taken as the average between the time-ratio and time-integral approaches) as a function of the donor-to-acceptor labelling ratio, we estimate 99% of the conA is clustered at the limit of infinite acceptor-to-donor labelling ratio (i.e. from the *y*-intercept of a clustered fraction versus donor–acceptor ratio plot).

Other cell-surface distribution models that could potentially account for the data include random distribution and a homogenous clustered distribution (Kenworthy and Edidin 1998). The random distribution can be excluded based on two observations. First, the calculated theoretical average energy-transfer efficiency based on a random surface distribution is significantly lower than the measured efficiency (Szollosi et al. 2002). On this basis, Szollosi et al. suggested that conA was partially clustered on the cell surface at an effective surface density that was higher than that expected for random distribution. Second, the acceptor-detected photobleaching kinetics are unaffected by increases in acceptor-labelling density (Kenworthy and Edidin 1998). Any random distribution would produce a decrease in *both* the donor- and the acceptor-detected photobleaching kinetics with increased acceptor density. This was not observed. We conclude that the conA receptors are nonrandomly organised (even if located in domains of high local concentration on the cell surface). A homogenously clustered model would be compatible with the disparate donor and acceptor photobleaching kinetics and the response of these to changes in acceptor-to-donor labelling ratio (Kenworthy and Edidin 1998). In this situation, the fractional population of molecules not undergoing FRET represents the population fraction of oligomers containing donor labels but not acceptor labels. However we could not conceive of any single oligomeric state that would yield the observed population fractions at the labelling ratios used. Thus, a partially clustered or a distributed oligomeric-state model is seen to be the simplest cell surface distribution consistent with the results herein.

Comparison with other studies

The distribution of conA on the surface of a variety of cell lines has been studied using a range of complementary techniques including microscopic and flow cytometric studies (Fernandez and Berlin 1976; Chan et al. 1979; Szollosi et al. 1984; Young et al. 1994; Cohen-Kashi et al. 2002). FRET efficiencies in the 25–60% range have been reported for conA-fluorescein and conA-rhodamine using steady-state fluorescence spectroscopy in normal and transformed murine fibroblasts ($E = 49\%$, A:D molar ratio = 5:1, Fernandez and Berlin 1976); donor-photobleaching fluorescence microscopy with murine B lymphocytes ($E = 49\%$, A:D molar ratio = 4:1, Young et al. 1994); donor-polarization-detected FRET microscopy using human T-lymphocyte cells ($E = 25\%$, A:D molar ratio = 4:1, Cohen-Kashi et al. 2002); and flow cytometry with HK22 murine lymphoma cells ($E = 57\%$, Chan et al. 1979; $E = 35\%$, A:D molar ratio = 4.3, Szollosi et al. 1984). Our transfer efficiency values for LIM1215 human colon carcinoma cells determined using donor photobleaching ($E = 31\%$, A:D molar ratio = 1.5:1; $E = 50\%$, A:D molar ratio = 3:1) are in the range of the reported values for other cell types. The variation in transfer-efficiency values obtained from these studies probably reflects the different cells used, the different methods used to determine the transfer-efficiency values, and the different reagent labelling ratios.

St. Pierre and Petersen (1990), using the technique of scanning correlation spectroscopy, have shown that the conA distribution is not homogenous but is compatible with a partly aggregated system consisting of monomers or small oligomers of high conA affinity and larger aggregates that bind conA with low affinity. If we assume that the high affinity monomers observed by St. Pierre are unable to undergo FRET, then the fraction-clustered protein obtained in our FRET analysis should agree with other approaches. In this regard, it is interesting to note that our estimates of clustered fraction of 87–99% (by extrapolation) agree well with the fraction of low-affinity binding sites from binding analysis (94%, Wallach 1976; 99%, Feller 1977). The good agreement in conclusions reached from three complementary approaches gives credence to the extended FRET method developed here.

As far as we are aware, this is one of the first FRET methods that has the potential to disentangle the effects of monomer–oligomer association from oligomer rearrangement in living cells. Monomer–oligomer dissociation would increase the proportion of non-FRET species as inferred from a change in donor-emission-detected FRET (but no change in acceptor-detected FRET), while oligomer rearrangement would be observed by a change in the acceptor-detected FRET.

Mekler and co-workers (1997) have used acceptor-sensitized photobleaching measurements to measure the distance distribution of probes in molecular assemblies. In essence they measured the depletion of acceptors due to indirect photobleaching from energy transfer from the excited donors. The approach requires a photostable donor and photolabile acceptor. Our approach differs in that we use the sensitized-acceptor emission to measure the kinetics of depletion of donors within molecules that are undergoing FRET within a photolabile-donor/photostable-acceptor system.

Other workers have attempted to use stoichiometry-based analysis methods, but the interpretation necessarily assumes that the transfer efficiency within the FRET population is a constant and any variation in observed average efficiency is due to a change in the relative proportion of FRET and non-FRET forms. This assumption is implicit in ratiometric methods (Hoppe et al. 2002) and has been used in interpreting data obtained from donor-detected photobleaching and lifetime measurements (Gadella and Jovin 1995). The use of the emission kinetics of the acceptor provides a direct kinetic measurement of the transfer efficiency in the oligomeric population and this provides an independent measurement of the transfer efficiency that is not biased by any free unassociated protein.

The method introduced here has advantages compared to other microscope-based FRET methods published in the literature; methods based on combined donor–acceptor intensity measurements using two or three filter sets are simple to perform but require careful corrections due to filter cross talk and direct excitation of the acceptor (Gordon et al. 1998). Moreover only an apparent efficiency is obtained which is necessarily dependent on labelling stoichiometry and proportion of monomeric receptors. The technique introduced here, while also requiring comparison of donor and acceptor intensities within a photobleaching series, has two distinct advantages. First, it is a kinetic measurement and hence less dependent on absolute signal than the intensity-based measurements. Second, only one cross-talk correction is required (donor bleed-through to the FRET channel) as opposed to three corrections required for intensity-based determinations. Direct excitation of the acceptor will contribute to the absolute intensity of the FRET channel but will not contribute to the FRET channel kinetics provided it is relatively photostable compared to the donor. Third, it has been suggested that combined donor–acceptor detection gives FRET data that is more reliable than using either channel separately (Berney and Danuser 2003).

Photobleaching FRET is inherently photodestructive, is potentially phototoxic, and can be relatively slow, suggesting that the technique is best used with fixed samples. We observed slight lateral cell movement during some of our live-cell experiments. This can be partially compensated using the time-ratio method introduced here involving collection and analysis of only a few images obtained over a relatively short time period. For example, good image registration is seen between the images collected consecutively in Fig. 2b, allowing the potential for ''on-the-fly'' FRET-imaging measurements in dynamic live-cell situations. As for other FRET techniques employing combined donor–acceptor emission, the photobleaching method employing dual-channel detection will work best for intermediate transfer efficiencies. At the limit of zero transfer efficiency, the amount of sensitized emission will be too small to detect, and at the limit of 100% efficiency the rate of photobleaching by direct or indirect excitation of acceptors will be comparable to the loss of sensitized emission due to loss of excitable donors. For the FITC/TRITC couple, this situation arises when the efficiency of transfer is 93%.

Work is in progress to further develop the method and theory for subcellular imaging and apply it to problems of importance in signal transduction. The newly developed quantum dot semi-conductor nanocrystals (Jovin 2003 and references therein) show some promise in this regard because their resistance to photobleaching and their large absorption cross section make them favourable acceptor candidates for the approach discussed herein.

References

Bastiaens PIH, Jovin TM (1996) Microscopic imaging tracks the intracellular processing of a signal transduction protein: fluorescent-labeled protein kinase C βI. Proc Natl Acad Sci USA 93:8407–8412

Bastiaens PIH, Majoul IV, Verveer PJ, Soling HD, Jovin TM (1996) Imaging the intracellular trafficking and state of the AB5 quaternary structure of cholera toxin. EMBO J 15:4246–4253

Berney C, Danuser G (2003) FRET or no FRET: a quantitative comparison. Biophys J 84:3992–4010

Chan SS, Arndt-Jovin D, Jovin TM (1979) Proximity of lectin receptors on the cell surface measured by fluorescence energy transfer in a flow system. J Histochem Cytochem 27:56–64

Clegg RM, Murchie AI, Zechel A, Lilley DM (1993) Observing the helical geometry of double-stranded DNA in solution by fluorescence resonance energy transfer. Proc Natl Acad Sci USA 90:2994–2998

Cohen-Kashi M, Moshikov S, Zurgil N, Deutsch M (2002) Fluorescence resonance energy transfers measurements on cell surfaces via fluorescence polarization. Biophys J 83:1395–1402

dos Remedios CG, Moens PD (1995) Fluorescence resonance energy transfer spectroscopy is a reliable ''ruler'' for measuring structural changes in proteins: dispelling the problem of the unknown orientation factor. J Struct Biol 115:175–185

Feller M, Richardson C, Behnke WD, Gruenstein E (1977) High and low affinity binding sites for concanavalin A on normal human fibroblasts in vitro. Biochem Biophys Res Commun 76(4):1027–1035

Fernandez SM, Berlin RD (1976) Cell surface distribution of lectin receptors determined by resonance energy transfer. Nature 264:411–415

Gadella TW Jr, Jovin TM (1995) Oligomerization of epidermal growth factor receptors on A431 cells studied by time-resolved fluorescence imaging microscopy: a stereochemical model for tyrosine kinase receptor activation. J Cell Biol 129:1543–1558

Gordon GW, Berry G, Liang XH, Levine B, Herman B (1998) Quantitative fluorescence resonance energy transfer measurements using fluorescence microscopy. Biophys J 74:2702–2713

Hirschfeld T (1976) Quantum efficiency independence of the time-integrated emission from a fluorescent molecule. Appl Opt 15:3135–3139

Hoppe A, Christensen K, Swanson JA (2002) Fluorescence resonance energy transfer-based stoichiometry in living cells. Biophys J 83:3652–3664

Jares-Erijman EA, Jovin TM (2003) FRET imaging. Nat Biotechnol 21:1387–1395

Jovin TM (2003) Quantum dots finally come of age. Nat Biotechnol 21:32–33

Jovin TM, Arndt-Jovin DJ (1989) FRET microscopy: digital imaging of fluorescence resonance energy transfer. Application in cell biology. In: Kohen E, Hirschberg JG, Ploem JS (eds) Cell structure and function by microspectrofluorometry. Academic Press, London, pp 99–117

Kenworthy AK, Edidin M (1998) Distribution of a glycosylphosphatidylinositol-anchored protein at the apical surface of MDCK cells examined at a resolution of < 100 Å using imaging fluorescence resonance energy transfer. J Cell Biol 142:69–84

Klostermeier D, Millar DP (2001–2002) Time-resolved fluorescence resonance energy transfer: a versatile tool for the analysis of nucleic acids. Biopolymers 61:159–179

Kubitscheck U, Schweitzer-Steiner R, Arndt-Jovin DJ, Jovin TM, Pecht I (1993) Distribution of type I Fc_{ϵ}-receptors on the surface of mast cells probed by fluorescence resonance energy transfer. Biophys J 64:110–120

Mekler VM, Averbakh AZ, Sudarikov A, Kharitonova OV (1997) Fluorescence energy transfer-sensitized photobleaching of a fluorescent label as a tool to study donor-acceptor distance distributions and dynamics in protein assemblies: studies of a complex of biotinylated IrM with streptavidin and aggregates of concanavalin A. J Photochem Photobiol B Biol 40:278–287

Millar DP (2000) Time-resolved fluorescence methods for analysis of DNA-protein interactions. Methods Enzymol 323:442–459

Selvin PR (2000) The renaissance of fluorescence resonance energy transfer. Nat Struct Biol 7:730–734

St. Pierre PR, Petersen NO (1990) Relative ligand binding to small or large aggregates measured by scanning correlation spectroscopy. Biophys J 58:503–511

Stryer L, Haugland RP (1967) Energy transfer: a spectroscopic ruler. Proc Natl Acad Sci USA 58:719–726

Sykes JA, Moore EB (1959) A new chamber for tissue culture. Proc Soc Exp Biol Med 100:121–127

Szollosi J, Tron S, Damjanovich S, Helliwell SH, Arndt-Jovin D, Jovin TM (1984) Fluorescence energy transfer measurements on cell surfaces: a critical comparison of steady-state fluorometric and flow cytometric methods. Cytometry 5:210–216

Szollosi J, Nagy P, Sebestyen Z, Damjanovich S, Park JW, Matyus L (2002) Applications of fluorescence resonance energy transfer for mapping biological membranes. Rev Mol Biotechnol 82:251–266

Wallach DF, Schmidt-Ullrich R (1976) Low- and high-affinity concanavalin A binding to thymocyte plasma membrane vesicles. J Cell Physiol 89(4):771–774

Whitehead RH, Macrae FA, St John DJ, Ma J (1985) A colon cancer cell line (LIM1215) derived from a patient with inherited nonpolyposis colorectal cancer. J Natl Cancer Inst 74:759–765

Young RM, Arnette JK, Roess DA, BG Barisas (1994) Quantitation of fluorescence resonance energy transfer between cell surface proteins via fluorescence donor photobleaching kinetics. Biophys J 67:881–888